Printed in the Republic of Korea

ANALYTICAL SCIENCE & TECHNOLOGY

Vol. 38 No. 3, 183-194, 2025

https://doi.org/10.5806/AST.2025.38.3.183

Comprehensive characterization and analysis of superabsorbent polymers for dehumidification systems: insights from polynomial regression, BET analysis, and FTIR

Onkar A. Dhumal★ and C. S. Choudhari

Department of Mechanical Engineering, All India Shri Shivaji Memorial Society, College of Engineering, Savitribai Phule Pune University, Pune-411001, Maharashtra, India

(Received February 25, 2025; Revised March 27, 2025; Accepted April 24, 2025)

Abstract: This study aims to explore sodium polyacrylate (SP) as a promising material along with silica gel for improving desiccant cooling systems through composite structures. This experimental investigation examines the pore characteristics and moisture adsorption capabilities of sodium polyacrylate (SP) samples with varying mesh sizes for potential use in dehumidification applications. The specimens were characterized by their unique surface area, total pore volume, and average pore diameter. The research employed Brunauer-Emmett-Teller (BET) methods alongside Fourier-transform infrared (FTIR) spectroscopy to elucidate key functional groups that improve moisture retention and to investigate the pore size distribution while considering the adsorption isotherms of superabsorbent polymers (SAP). The results showed mesoporous structures in all samples, with SP1 showing a pronounced hysteresis loop, suggesting significant capillary condensation. SP1's high pore volume and mesoporous nature make it suitable for applications requiring high moisture uptake and retention. The adsorption energy for SP3 exhibits a 20.79 % elevation in comparison to that of SP1 and SP2, thereby suggesting an augmented adsorption energy at elevated relative pressure conditions.

Key words: sodium polyacrylate, adsorption capacity, superabsorbent, dehumidification

Nomenclature:

g_w/g_{ads}	adsorption capacity
g_w	mass of adsorbate
g_{ads}	gram of adsorbent
wt%	weight-percentage
σ	molecular cross-sectional area
pH	potential of hydrogen
cc	cubic centimeters
Å	angstrom
W	amount adsorbed by adsorbate
W_m	monolayer capacity
P/P_0	relative pressure
P	equilibrium pressure
P_0	saturation pressure

★ Corresponding author
Phone : +91-989-030-4191
E-mail : onkar.dhumal@gmail.com

1. Introduction

Systems for dehumidification that can efficiently control humidity and temperature hold promise as a way to address future energy consumption issues while taking human comfort into account. It is important to choose the right desiccant materials for desiccant-based cooling systems to work well overall, even though most research has focused on comparing different desiccant materials and composite compositions. Materials including activated alumina, natural zeolite, silica gel, molecular sieves, and synthetic polymers have all been thoroughly investigated as solid desiccants for dehumidification and humidification applications.

Desiccant-based dehumidification systems use low-quality heat sources for regeneration, but their practical uses are limited by their high initial costs and inefficient performance. Along with the identified advanced materials, significant research should concentrate on enhancing performance, dependability, and cost-effectiveness.[1] In order to address problems and suggest further study for improved performance, analysis looks at performance measures, desiccant air conditioner operations, and novel materials.[2] The greatest results and temperature-related acceleration of water outflow were obtained from a study on the Scheffler reflector with activated alumina, silica gel, and a molecular sieve for desiccant replenishment.[3] Silica gel performs better than molecular sieves and activated alumina, and raising the bed's temperature speeds up the water's release.

Hygroscopic polymers offer greater capabilities for both sorption and desorption of moisture in solid desiccant cooling (SDC) systems. A systematic evaluation was conducted on three distinct composite materials to ascertain their efficacy in air dehumidification in comparison to desiccant wheels composed of silica gel: lithium chloride, a blend of silica gel and molecular sieve 5A, and a composite integrating silica gel, lithium chloride, and molecular sieve 5A. The recorded adsorption and regeneration rates for the composite and silica gel desiccant wheels were found to be 34.99 %, 43.58 %, and 85.5 % superior, respectively.[5]

The employment of thermo-reactive super-porous gels (SPGs) made from acrylamide (AM) and N-isopropylacrylamide (NIPAM) could potentially replace standard solid desiccants. Following their production through gas blowing and foaming techniques, the surface morphology of the SPGs was rigorously analysed employing scanning electron microscopy (SEM). The maximum adsorption capacity of the isotherm was ascertained to be adsorption capacity of 0.75 g·w/g·ads at a temperature of 25 °C and a relative humidity of 90 %, thereby categorizing it as type-III. The SPGs demonstrated favourable regeneration and reusability across ten consecutive adsorption/desorption cycles.[6]

To formulate a composite material intended for utilization in air conditioning systems, silica gel is combined with sodium polyacrylate and polyacrylic acid. The optimal mixing ratio was 10:1:1.[7] The sorption capacity of the material rose by 41 % at 25 °C and 25 % humidity. After 15 minutes under various circumstances, it continued to dehumidify at an average rate of 2.73 g/min, maintaining 80 % of its maximal capacity. S2-EG500 improves thermal conductivity by 2.8 times over SGP in the study of water vapor adsorption properties on silica gel-based composites using HEC, PVA, PVP, and gelatin binder types. The study found that SGP composite with 2 wt% PVP outperformed the others in terms of its porosity and thermal properties. The composite demonstrated a 12.5 % increase in adsorption uptake, suggesting that it is appropriate for the construction of high-performance adsorption cooling systems.[8,9]

To produce superabsorbent polymers (SAPs), blends of CMC/AAc and PVA/AAc were polymerized in an aqueous solution. The CMC/AAc combination had the greatest swelling capacity, according to a comparison analysis. N, N'-methylenebisacrylamide cross-linker caused the gel fraction to decrease, although the amount of benzoyl peroxide increased the water adsorption capacity by.[10] In terms of heat and mass transfer, two novel silica-based consolidated composite adsorbents outperformed silica gel by a significant margin.[11] To produce silica gel augmented with

carbon fiber powder and carboxymethyl cellulose (CMC), researchers used freeze-drying.

Two new desiccants that improve the desiccant wheel regeneration efficiency at low temperatures are zeolite and superabsorbent polymer.[12] The superabsorbent polymer wheel outperformed the zeolite wheel in terms of dehumidification. A new silica gel-based desiccant chemical was introduced that can be used for coatings, sheets, and monolithic components. Good mechanical and stability characteristics were demonstrated by the small-scale prototype.[13]

Using four distinct new samples made of HCl, $(NH_4)2CO_3$, and $CaCl_2$, as well as the composition of sodium polyacrylate (SP), the efficacy of adsorption systems is investigated. The system may function effectively if it is powered by geothermal energy, waste heat, or renewable energy. The results showed that the composite composed of SP/$CaCl_2$ had the highest adsorption uptake.[14]

The study on Si_2/Al_2O_3 geopolymers indicated that the toughness correlates with the SiO_2 to Al_2O_3 ratio, affecting both the material's mechanical traits and microstructural attributes. The influence of organic polymers on these properties and microstructures was examined utilizing varying Si_2/Al_2O_3 ratios.[15] The data shows that the relationship between SiO_2 to Al_2O_3 substantially affects the polymer's role in defining the mechanical traits of metakaolin geopolymer, with the impact decreasing when the ratio is heightened. It is specifically the geopolymers that possess a lower Si_2/Al_2O_3 ratio which can experience a notable transformation through the toughening impact of the organic polymer on the geopolymer.

A composite material synthesized from organo-bentonite and sodium polyacrylate was incorporated into mortar to formulate OBT/PAAS humidity-regulating cementitious mortars. The mortar was evaluated with Fourier-transform infrared spectroscopy (FTIR), X-ray diffraction (XRD), environmental scanning electron microscopy (ESEM), and Brunauer-Emmett-Teller (BET) analysis, uncovering improved morphology and humidity handling skills. Furthermore, the mortar exhibited an increased specific surface area and pore volume. Within a desiccator environment, the prepared and solidified OBT-PAAS mortar was capable of maintaining relative humidity levels between 38 – 62 RH%.[16] The Super Desiccant Polymer (SDP) was additionally proposed due to its exceptional adsorption efficiency and durability.[17] The simulation of the system was executed using *Comsol* software, supported by an experimental database for validation purposes. With a coefficient of performance (COP) value of 1.1, the SDP desiccant wheel demonstrates superior efficacy compared to alternative air conditioning desiccant systems in Gabes, Tunisia, showcasing its enhanced performance across various operational conditions. A self-moisture-absorbing hydrogel polyacrylate film has been innovatively developed for hybrid passive cooling, effectively diminishing solar heating while optimizing thermal emission, thereby contributing to a reduction in global carbon emissions by 5 °C.[18] In contrast to traditional dehumidification methodologies associated with a desiccant wheel, a regeneration technique employing a composite of silica gel and polymer, utilizing heat sourced from a heat pump, exhibited a remarkable performance enhancement of 130 %.[19]

The architectural framework of Superabsorbent Polymer (SAP) alongside the mechanisms governing water adsorption was meticulously analyzed, focusing on critical components and methodologies for enhancing operational efficacy, including the elevation of SAP concentration, reusability, salinity resilience, and water adsorption capabilities.[20] Employing controlled hydration conditions within regulated environments, a hygroscopic methodology was developed to assess the sorption characteristics of porous materials.[21] The high-resolution data generated through this methodology is vital for understanding complex pore structures. The application of SAP in maize dryers was utilized to accelerate drying processes; however, its propensity for swelling and subsequent solidification may detract from its functional utility and potentially inhibit rewetting under conditions of elevated humidity during storage.[22]

To address the limitations associated with traditional desiccants such as silica gel and zeolites, and to enhance adsorption capacity along with desorption

rate coefficients, a novel polymer material was introduced for use within desiccant wheels.[23] In comparison to silica gel, the polymer material exhibited an improvement of 17 – 53.9 %, particularly under conditions of low relative humidity. The exploration of environmentally sustainable desiccant materials including polylactic acid (PLA), pine wood combined with PLA (PW-PLA), and olive pit integrated with PLA (OP-PLA) for the purpose of constructing and evaluating a 3D printed desiccant system was also undertaken.[24] Notably, PW-PLA demonstrated an adsorption capacity that was up to 12.7 % superior to that of OP-PLA, indicating its optimal performance. The system's minimal pressure differentials coupled with adequate moisture extraction capabilities suggest its viability for dehumidifying ambient air.

Desiccant systems face reliability challenges due to extended operation. Further research is needed to improve longevity and create stronger materials. While cutting-edge materials like super porous gels and metal-organic frameworks have been explored, more research is needed to discover novel materials with greater effectiveness.

This study aims to investigate the physical adsorption characteristics of the selected materials to identify the best suitable material in composition with traditional desiccant materials. Methodology for the investigation is selected based of physisorption characterization of superabsorbent materials. In this work, sodium polyacrylate (SP) introduced as a superabsorbent to address the aforementioned issues. sodium polyacrylate (SP) can be used to build various desiccant-based composites that can be employed in coatings, monolithic components, and desiccant technologies. Due to its considerable manufacturing flexibility, the adsorbent product's performance and geometry may be tailored to meet specific industrial constraints, making it a valuable addition that can be used in a variety of application situations. Fourier Transform-Infrared Spectroscopy (FTIR) analysis and the Brunauer-Emmett-Teller (BET) test have been used to examine the adsorption, structural stability, and thermal stability of SP samples.

2. Materials and Methods

2.1. Materials

The superabsorbent sodium polyacrylate (SP) utilized in the experiment was chemically pure and obtained from Chemzest Pvt. Ltd. (Chennai, India). Sodium polyacrylate, known for its high absorbency, can retain water many times its weight and is employed in various consumer products. This chemical polymer, with the formula $C_3H_3NaO_2$, is recognized as a significant and innovative functional material. The solid form appears as a white powder, and its synthetic variant is incorporated into cosmetics and personal hygiene items due to its ability to absorb up to 500 times its weight in water. Primarily functioning as a thickening agent, it retains its white powder form when dry and transforms into a gel-like state upon hydration. The monomer for polyacrylate originates from acrylic acid, represented by the simplified structure CH_2=CHCOOH. Through the process of addition polymerization, the double bond in acrylic acid forms extensive polymer chains. The resulting

SP1 (50-25 mesh) SP2 (85-50 mesh) SP3 (230-100 mesh)

Fig. 1. Sodium Polyacrylate with varying mesh size.

Table 1. Physical characteristics of SPs

Characteristics	SP1	SP2	SP3
Particle Size	50 – 25 mesh	85 – 50 mesh	230 – 100 mesh
Adsorption Speed (g/g·s)	≤45	≤70	≤80
pH Value	7.0 – 8.0	6.0 – 7.0	5.6 – 6.5
Appearance	White Fine Granular	White Fine Granular	White fine powder

sodium polyacrylate features sodium ions (Na^+) linked to the carboxylate groups (COO-) within the polymer chain, leading to both two-dimensional and interactive three-dimensional structures.

The sodium polyacrylate (SP) samples used for this study are displayed in *Fig.* 1 with different mesh sizes. These will be used to determine the adsorption capacity, adsorption/desorption cycles, and surface area significance. *Table* 1 displays the properties of sodium polyacrylate. The chemical properties of sodium polyacrylate with particle sizes of 50 – 25 mesh (SP1), 85 – 50 mesh (SP2), and 230 – 100 mesh (SP3) was compared for adsorption phenomena. The porosity and surface area of sodium polyacrylate are influenced by the particle size. Higher adsorption capabilities may arise from the increased surface area of finer particles. Faster adsorption rates are frequently the result of smaller particle sizes. The ability of sodium polyacrylate to absorb and retain large amounts of water is well known. The pH of the surrounding environment has an impact on sodium polyacrylate's swelling behavior. In alkaline conditions as opposed to acidic ones, the polymer might swell more.

One important factor in many applications is the adsorption speed, or the rate at which sodium polyacrylate absorbs and holds onto water. Increased adsorption speed is important for SPs because it promotes rapid adsorption, improved liquid retention, and the kinetics of water adsorption and subsequent release.

2.2. Methods

2.2.1. Brunauer-emmett-teller (BET) test

Chemical investigations of powdered samples assessed the structural stability of superabsorbent materials. Water adsorption isotherms and linear isotherms were quantified using a BET apparatus (Autosorb iQ Station 2).

In order to eradicate moisture and volatile contaminants, the samples, with an identified mass, underwent a meticulous outgassing procedure for a duration of 2.1 hours at a temperature of 200 °C. Helium (He) was employed to ascertain the void volume, and the analytical methodology is considered standard within the field. In this examination, Nitrogen (N_2) is noted for its molecular weight of 28.013 g/mol and functions as the adsorbate gas. The temperature of the bath, corresponding to the liquid nitrogen phase, is established at 77.35 K when the analysis gas is determined to be nitrogen. The effective molecular diameter is quantified to be 3.54 Å. During the adsorption procedure, nitrogen gas is systematically introduced into the sample chamber at controlled pressures. The adsorbed volume is quantified at varying relative pressures (P/P_0), where P denotes the applied pressure and P_0 represents the saturation pressure of nitrogen. The desorption curve is generated by incrementally reducing the pressure and subsequently monitoring the volume of nitrogen that has been desorbed from the surface.

The BET methodology consists of a dual-phase procedural application. In the initial phase, a physisorption isotherm is converted into a "BET plot" for the purpose of quantifying the BET monolayer capacity, Wm. Monolayer capacity pertains to the quantity of adsorbate that can be accommodated within a completely saturated single molecular layer on the unit mass surface. In the subsequent phase, the cross-sectional area of the molecule, σ, is ascertained to compute the BET-area, a (BET), based on Wm. Generally, the BET Eq. (1) is employed in its linear representation.

$$\frac{1}{W\left[\left(\frac{P_0}{P}\right)-1\right]} = \frac{1}{W_m \cdot C} + \frac{C-1}{W_m \cdot C}\left(\frac{P}{P_0}\right) \tag{1}$$

where P/P_0 represents the relative pressure, W_m denotes the mass of the monolayer adsorbate, C indicates the BET constant, and W pertains to the mass of the adsorbed gas. The BET theory posits an exponential relationship between the constant C and the energy associated with the adsorption of the monolayer. The exponential factor relating to the adsorption heat of the adsorbate on the adsorbent is the determinant of the C-value within the context of the BET framework. The isotherm graph formulated according to the parameters established by BET can be effectively interpreted through the C value.

The slope, S (Eq. (2)) and y-intercept, I (Eq. (3)) can be obtained using least squares regression.

$$S = \frac{C-1}{W_m \cdot C} \tag{2}$$

And

$$O = \frac{1}{W_m \cdot C} \tag{3}$$

The monolayer capacity W_m can be calculated with following equation (Eq. (4))

$$W_m = \frac{1}{S+I} \tag{4}$$

Once W_m is determined, the total surface area S_t can be calculated with the following equation;

$$S_t = \frac{W_m \cdot N \cdot A}{M} \tag{5}$$

where N represents Avogadro's constant, A denotes the cross-sectional area of the adsorbate, which is quantified as 0.162 nm² for a nitrogen molecule that has been absorbed, and M signifies the molar volume.

Moreover, a methodology utilized for the characterization of the surface area of porous substances, which yields critical insights regarding their porosity and adsorption characteristics, is referred to as the multipoint BET (Brunauer-Emmett-Teller) method. Its importance is underscored by its capacity to evaluate surface area with enhanced accuracy in comparison to the single-point BET technique. The Multi-Point BET method functions within a relative pressure spectrum ranging from 0.1 bar to 0.5 bar.

The performance of SPs in absorbing liquid solutions is heavily affected by characteristics like pore volume, pore diameter, and the specific surface area of sodium polyacrylate. The term pore volume refers to the volume of vapor that is adsorbed at a relative pressure of one. Pore dimensions, ascertained by the average pore radius, categorize materials into mesoporous, microporous, or macroporous classifications. Both pore volume and dimensions significantly influence the specific surface area, thereby augmenting the material's adsorption potential, which is delineated as the unit mass of the adsorbent (e.g., sodium polyacrylate).

2.2.2. Adsorption Isotherm of SAP

Understanding adsorption isotherms is crucial for interpreting and defining the pathways through which a certain substance attaches to a solid backing. Such isotherms provide critical insights into the nature of the interactions that occur between the adsorbent surface, the locus of adsorption and the adsorbate, or the material undergoing the adsorption process. Researchers can estimate crucial adsorbent characteristics like surface area and porosity by examining adsorption isotherms. For instance, specific surface area is determined using multilayer adsorption isotherms in BET (Brunauer, Emmett, and Teller) theory.

The mechanics of adsorption are revealed by many adsorption isotherm models, such as Freundlich and Langmuir. The Langmuir isotherm suggests the occurrence of monolayer adsorption on a uniform surface, while the Freundlich isotherm accommodates multilayer adsorption on a non-uniform surface. Understanding adsorption isotherms is vital for figuring out the highest amount of substance that an adsorbent can capture, which is important for practical uses including gas separation, water treatment, and catalytic processes.

Instead of mesoporous or microporous materials, sodium polyacrylate usually displays adsorption isotherms that are linked to non-porous or macroporous materials. According to IUPAC guidelines, Freundlich or Langmuir isotherms frequently provide a more accurate description of the adsorption behavior of sodium polyacrylate.[25]

The Freundlich isotherm is frequently applied to non-ideal adsorption and heterogeneous surfaces. Its expression can be found in Eq. (6).

$$Q = K \cdot C^n \tag{6}$$

In this scenario, C indicates the level of concentration of the adsorbate at equilibrium, K is a constant, n is characterized as an empirical figure, and Q represents the total volume of adsorbate that has adhered to the mass of the adsorbent.

Commonly, the Langmuir isotherm is utilized to clarify how adsorbate forms a monolayer on a surface defined by a restricted number of equivalent positions. The formulation of this isotherm is articulated in Eq. (7).

$$Q = \frac{Q_{max} \cdot K \cdot C}{1 + K \cdot C} \tag{7}$$

C is the measure of adsorbate concentration at equilibrium, Q_{max} indicates the maximum capacity for adsorption, K is the Langmuir constant, and Q refers to the total quantity of adsorbate that has been absorbed onto a specific mass of adsorbent.

It's crucial to remember that the particular isotherm that best captures sodium polyacrylate's adsorption behavior may vary depending on the adsorbate's characteristics and the experimental setup. Finding the best model for a particular set of circumstances can be aided by fitting to these isotherms and using experimental data.

2.2.3. Fourier transform Infrared (FTIR) spectroscopy

A Fourier Transform Infrared (FTIR) Spectroscopy investigation was performed on a few chosen materials in order to determine which functional groups were superabsorbent at the adsorption position (cm^{-1}, wavenumber) for relative adsorption intensity. With an accuracy and precision of <0.05 cm^{-1} @ 1576 cm^{-1} and <0.0005 cm^{-1} @ 1576 cm^{-1}, respectively, the FTIR instrument (ALPHA II, Bruker) generates data with spectra ranging from 500 to 4000 cm^{-1}, wavenumber.

In this study, sodium polyacrylate's molecular structure and chemical makeup are determined using FTIR. Chemical identification based on polymer structure and function group provides important details about a chosen substance. Functional group characterization is specifically dependent on the presence of carbonyl and acrylic acid groups. The Central Instrumentation Facility at SPPU, State University, India, provided all test facilities.

3. Results and Discussion

The performance of sodium polyacrylate (SPs) in adsorbing liquid solutions is heavily affected by characteristics like pore volume, pore diameter, and the specific surface area of sodium polyacrylate. The term pore volume refers to the volume of vapor that is adsorbed at a relative pressure of one. Additionally, beyond improving our comprehension of sodium polyacrylate's attributes and opening up new research directions, the chapter prompts readers to examine the detailed nature of the material and its possible applications across scientific and industrial sectors.

3.1. Characterization of pore structure of superabsorbent

The characteristic pore properties of SPs are listed in *Table* 2. Applications needing a large pore volume and a fairly high specific surface area can use SP1 (50 – 25 mesh). For situations requiring a high surface area with numerous tiny pores, SP2 (85 – 50 mesh) is ideal. Systems that benefit from larger pores with a moderate pore volume and reduced surface area are best suited for SP3 (230 – 100 mesh). The surface area plays a critical role in the interactions between sodium polyacrylate and other constituents within a composite matrix. This factor can significantly influence compatibility, stability, and overall performance across diverse formulations. Consequently, it would be reasonable to predict that any alteration in the water-adsorption properties would similarly be expected.

3.2. Adsorption mechanism of sodium polyacrylate

The kinetic behavior associated with the adsorption

Table 2. Characteristic pore properties of SPs

Characteristics	SP1 (50 – 25 mesh)	SP2 (85 – 50 mesh)	SP3 (230 – 100 mesh)
Specific Surface Area (m^2/g)	0.633	0.637	0.508
Total Pore Volume (mm^3/g)	1.386	0.997	1.222
Average Pore Radius (Å)	4.377	3.139	4.814

of sodium polyacrylate may encompass both monolayer and multilayer adsorption phenomena, influenced by specific conditions and the fundamental characteristics of the adsorption process. Under conditions of low adsorbate concentrations, monolayer adsorption is likely to emerge as the dominant feature exhibited by sodium polyacrylate. This phenomenon is delineated by the formation of a unique monolayer of adsorbate molecules upon the surface of the adsorbent (polymer), a process referred to as monolayer adsorption. Such an occurrence is typically discerned during the initial stages of adsorption when the existing surface sites are insufficiently filled. Conversely, as the concentration of the adsorbate increases, sodium polyacrylate may undergo a transition towards multilayer adsorption. This multilayer adsorption entails the formation of additional layers of adsorbate that are superimposed upon the pre-existing monolayer. This advancement transpires as an increasing number of adsorbate molecules adhere to the surface, culminating in the establishment of multiple layers.

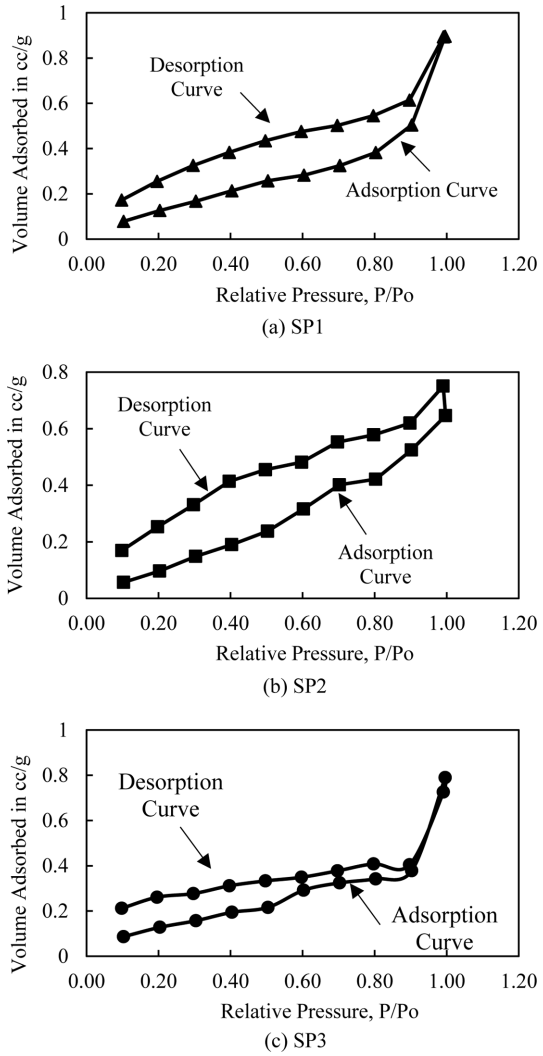

Fig. 2. N_2 adsorption and desorption isotherms of SP1 (a), SP2 (b) and SP3 (c).

Fig. 2 illustrates the N_2 adsorption isotherms for samples SP1, SP2, and SP3, which are associated with both adsorption and desorption curves. The N_2 adsorption isotherm for sodium polyacrylate samples (SPs) suggests the phenomenon of multimolecular layer adsorption. The limited quantity of adsorption observed at lower pressures signifies a suboptimal interaction between N_2 and the SPs. As relative pressure increases, the amount of N_2 adsorbed exhibits a corresponding increase. This indicates that N_2 molecules were effectively accommodated within the pores.

Fig. 2(a) shows the SP1 BET Isotherm wherein volume adsorbed shows characteristic Type IV isotherm behavior with a hysteresis loop suggestive of mesoporous materials; increases with relative pressure. A sharp increase in the desorption curve at increasing relative pressures indicates capillary condensation inside the mesopores. This behavior suggests that SP1 is a good candidate for adsorption applications due to its large surface area and mesoporous structure.

In case of SP2 the plot in *Fig.* 2(b) implicates that because of its smaller average pore radius, SP2's volume adsorbed is similar to SP1's, with a minor decrease in adsorption capacity. The persistence of the hysteresis loop in the desorption curve attests to the mesoporous structure. Though marginally less effective in terms of adsorption, SP2 is nevertheless viable because to its smaller pore size and reduced pore volume in comparison to SP1.

SP3 has the largest adsorption capacity of the three, as seen in *Fig.* 2(c), which is indicative of its bigger average pore radius and higher pore volume. The desorption curve has the biggest hysteresis loop, which

suggests a considerable mesoporosity and higher adsorption energy. Because SP3 can absorb more moisture, its greater hole radius and increased pore volume make it more suitable for dehumidification applications.

The BET equation meticulously establishes a linear relationship, as evidenced by the graph of $1/[W(P_0/P) - 1]$ plotted against P/P_0 for SP1, SP2, and SP3, utilizing nitrogen as the adsorbate. The BET equation clarifies the relationship between the quantity of gas molecules adsorbed (W) at a given relative pressure (P/P_0). The maximum limit of adsorbate that can be held on the surface is identified as the monolayer capacity.

In this investigation, the BET constant (C) provides valuable insights into the energy dynamics associated with the adsorption process. *Table* 3 provides an elevated value of C (23.682) indicates superior adsorption characteristics in SP3, compared to SP1, which has C = 8.659, and SP2, which possesses C = 4.715. In the context of the dehumidification process, a moderate BET constant value, also referred to as the energy of adsorption in conjunction with a mesoporous structure, represents a viable option alongside silica gel and other desiccants. A monolayer adsorption capacity of ~0.000182 g/g is the highest for SP2, followed by ~0.000181 g/g for SP1 and ~0.000145 g/g for SP3. Greater Wm indicates a larger surface area or more adsorption sites. Every sample has a high R^2 value (>0.98), indicating that the BET model provides a good fit to the data. At the relative pressure of $P/P_0 = 1$, SP2 demonstrates a maximum adsorption capacity that correlates with the interpretation of adsorption isotherm plots.

The curve of $1/[W(P_0/P) - 1]$ vs P/P_0 is displayed in *Fig*. 3, and *Table* 4 provides the BET adsorption data acquired during nitrogen adsorption on SPs. Based on the observed variations in the BET function values and the corresponding polynomial equations, it appears that SP1 possesses the most substantial surface area and potentially the greatest porosity among the three samples analyzed.

SP3's strong cubic regression trend suggests a nonlinear adsorption process, possibly due to steric hindrance, crosslinking density, or selective adsorption behavior. This behavior is advantageous for controlled adsorption applications, where a material selectively adsorbs moisture or contaminants rather than unregulated absorption.

Conversely, the surface areas and porosities of SP2 and SP3 are comparatively diminished. Perhaps the most effective is SP1, especially for applications like dehumidification that require a wide surface area and

Table 3. BET parametric analysis

SAP Samples	BET Monolayer Capacity (W_m)	BET Surface Area (S_t) (m^2/g)	BET Constant (C)
SP1	0.000181 g/g	0.633 m^2/g	8.659
SP2	0.000182 g/g	0.637 m^2/g	4.715
SP3	0.000145 g/g	0.508 m^2/g	23.682

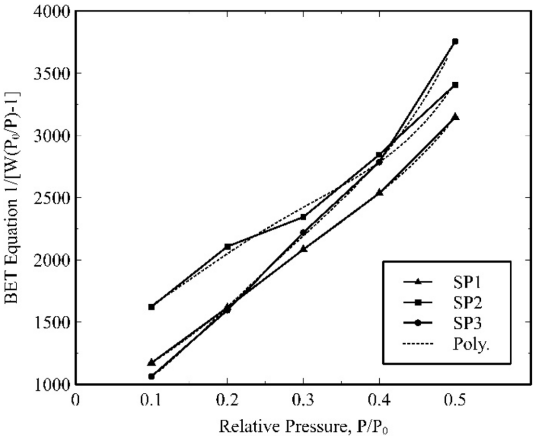

Fig. 3. $1/W((P_0/P) - 1)$ Vs Relative pressure P/P_0 plot of SPs

Table 4. Linear regression relation of SPs

SAP Samples	R square Value	Regression Correlation	R^2 (Goodness of Fit)
SP1	0.9997	y = 11533x3 − 8123.6x2 + 6234.3x + 615.1	0.9997
SP2	0.9961	y = 25867x3 − 20266x2 + 8603.7x + 949.36	0.9961
SP3	0.9988	y = 26117x3 − 17663x2 + 9232.5x + 281.64	0.9988

adsorption capacity. While SP2 and SP3 are still valuable, their applications may be better suited for situations where a modest surface area and sufficient porosity are required.

3.3. Fourier transform infrared spectroscopy (FTIR) analysis

Sodium polyacrylate (SP) can absorb water and swell because of its hydrophilic group. It is important to emphasize that the comprehensive adsorption capacity of sodium polyacrylate is affected by variables beyond mere functional groups that determine the polymer's architecture and crosslinking characteristics. The intricate interplay between the polymer and the adsorbate (for instance, water or other liquid substances) is contingent upon numerous factors, encompassing the polymer's holistic structure and chemical composition.

When interpreting FTIR spectra, the full spectrum should be taken into account, along with the existence and intensity of different peaks. Furthermore, experimental techniques tailored to the target application are frequently used to evaluate the adsorption capabilities of sodium polyacrylate.

Fig. 4. shows FTIR spectra of SPs. The prominent

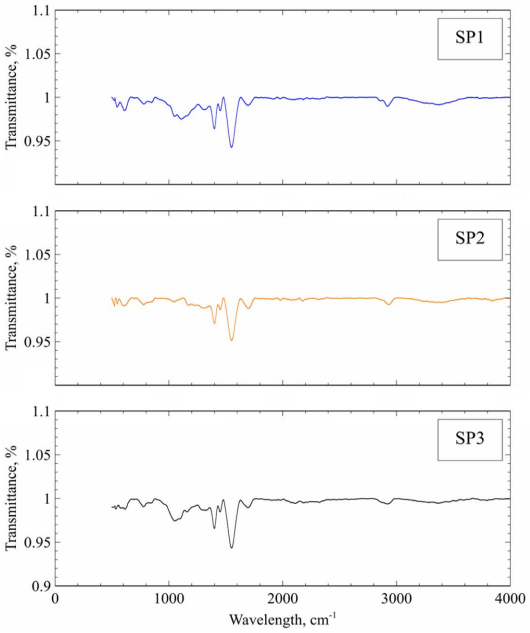

Fig. 4. FTIR Spectra of SPs.

adsorption band detected in the FTIR spectra of the SP1 powder, positioned at approximately 3372 cm^{-1}, is ascribed to the stretching vibrations of hydroxyl groups linked to the adsorbed water molecules. The broad intensity band, which is primarily situated at 1697 cm^{-1}, is predominantly affected by the scissoring vibrations of H_2O, thus concealing the C=O stretching band that is emblematic of carboxylic groups. The two adsorption bands observed at 1549 and 1399 cm^{-1}, respectively, signify the symmetric and asymmetric stretching vibrations associated with the carboxylate anion (–COO−). The bands identified at 2921, 1451, and 1310 cm^{-1} originate from the stretching and bending vibrations of CH_2 and CH, which are fundamental constituents of the aliphatic backbones. The extensive band centered at 2179 cm^{-1} results from the C=C=O stretching vibrations of the ketene functional group, whereas the broad band at 1913 cm^{-1} is ascribed to the C=C=C stretching vibrations characteristic of the allene functional group.

The FTIR spectra of SP2 exhibits a comparatively less pronounced band at 3845 cm^{-1} within the extended ultraviolet region. The FTIR spectrum of the powdered SP2 reveals nearly identical functional groups. Conversely, the spectral bands and both stretching and flexible vibrations correspond to those observed in SP1. In addition, FTIR spectra of SP3 features bands at 1158 and 1051 cm^{-1} indicative of C-F and C-O stretching vibrations characteristic of alcohol and fluoro-compounds.

The identification and intensity of the carbonyl functional group C=O within the Fourier Transform Infrared (FTIR) spectrum provide valuable insights into the acrylate moieties incorporated within the polymeric structure. This particular functional group is instrumental in facilitating interactions with water and may augment the polymer's adsorption capabilities. With a wavenumber of 1697.38 cm^{-1}, the C=O bond in sample SP1 differs from SP2, which has 1699.76 cm^{-1}, and SP3 at 1696.04 cm^{-1}. The results suggest that SP2 demonstrates a relatively robust C=O bond, which is suggestive of the superior adsorption efficacy characteristic of that particular superabsorbent polymer.

The disparities observed in peak intensity may be attributed to fluctuations in polymer packing density, which can subsequently influence hydrogen bonding and steric hindrance. SP1, SP2, and SP3 present varied crosslinking intensities, the peaks for carbonyl (C=O) and hydroxyl (O-H) reflect changes resulting from restricted molecular motion.

Sodium polyacrylate possesses a significant degree of hygroscopicity. Fluctuations in moisture content could result in subtle shifts or alterations in intensity concerning O-H stretching and carboxylate peaks. In the event that SP1, SP2, and SP3 present different mesh sizes, steric effects may elucidate minor displacements in peak positions and intensity variations within their FTIR spectra. Increased particle sizes (SP1 compared to SP3) may yield enhanced intermolecular interactions, leading to the broadening or shifting of peaks. Variations in steric hindrance could also influence water absorption, which in turn affects the peak intensities associated with hydroxyl and carboxylate groups.

4. Conclusions

A thorough experimental investigation was conducted employing a variable mesh size on commercially obtainable sodium polyacrylate, which is predominantly utilized as a super-adsorbent polymer. The evaluation of pore size distribution and adsorption properties, utilizing isotherms, produces noteworthy findings. The findings for SP1, SP2, and SP3 indicate a more favorable combination with desiccant materials for the formulation of composite materials utilized in desiccant technology. The specific conclusions obtained from this exploration are stated as follows:

- Strong Adsorption Sites: The elevated BET constant (C = 23.682) implies the existence of enhanced interactions with adsorbates compared to SP1 and SP2, thereby rendering SP3 (230 – 100 mesh) particularly efficacious in applications predicated on adsorption.
- Enhanced Functional Groups for Adsorption: SP3 shows slight shifts in peaks, suggesting higher crosslinking density, which could create well-defined micropores for enhanced adsorption. FTIR spectroscopic analysis reveals the presence of hydroxyl (-OH) (~3400 cm^{-1}) and carboxylate C=O stretching (~1700 cm^{-1}) and COO^- peaks (~1400 cm^{-1}) functional groups, which significantly augment the capacity for moisture and ionic adsorption.
- Predictable & Stable Adsorption Behavior: The high R^2 values alongside robust regression correlations signify a consistent and dependable performance profile for all samples, which is paramount for industrial applications involving adsorption.
- Selective Adsorption Potential: Although the BET surface area is comparatively diminished, the pronounced interaction indicated by the elevated C value by 20.79 % suggests that SP3 may provide a controlled and efficient mechanism for adsorption, especially concerning specific gases, moisture, or contaminants.
- SP3 emerges as the most appropriate super absorbent polymer (SAP) sample for adsorption applications, attributable to its robust interactions with adsorbates, selective adsorption capabilities, and high predictability.

Further use of SP3 in product development of polymer matric composite leads to remarkable enhancement in composite desiccant wheel used in desiccant cooling and dehumidification applications.

Conflict of Interest

We declare that we have no conflict of interest.

Acknowledgments

Central Instrumentation Facility, SPPU, State University, India.

References

1. M. M. Abd-Elhady, M. S. Salem, A. M. Hamed, and I. El-Sharkawy, *International Journal of Refrigeration*, **133**, 337-352 (2022). https://doi.org/10.1016/j.ijrefrig.2021.

09.028
2. M. Abdelgaied, M. A. Saber, M. M. Bassuoni, and A. M. Khaira, *Environmental Science and Pollution Research,* **30**, 28344-28372 (2023). https://doi.org/10.1007/s11356-023-25209-z
3. M. Safwan, A. Ramli, S. Misha, N. F. Haminudin, M. A. M. Rosli, A. A. Yusof, M. F. M. Basar, K. Sopian, A. Ibrahim, and A. F. Abdullah, *International Journal of Heat and Technology*, **39**(5), 1475-1482 (2021). https://doi.org/10.18280/ijht.390509
4. H. Liu, S. Sundarrajan, G. V. Kumar, and S. Ramakrishna, *Macromol. Mater. Eng.*, **308**(12), 2300176 (2023). https://doi.org/10.1002/mame.202300176
5. K. S. Rambhad, P. V. Walke, V. P. Kalbande, M. A. Kumbhalkar, V. W. Khond, Y. Nandanwar, M. Mohan, and R. Jibhakate, *SN Applied Sciences*, **5**, 277 (2023). https://doi.org/10.1007/s42452-023-05505-6
6. H. Mittal, A. Al Alili, and S. M. Alhassan, *Scientific Reports*, **12**, 5626 (2022). https://doi.org/10.1038/s41598-022-08191-3
7. C.-H. Chen, C.-Y. Hsu, C.-C. Chen, and S.-L. Chen, *Energy and Buildings*, **101**, 122-132(2015). https://doi.org/10.1016/j.enbuild.2015.05.009
8. M. M. Younes, I. I. El-sharkawy, A. E. Kabeel, K. Uddin, A. Pal, S. Mitra, K. Thu, and B. B. Saha, *International Journal of Refrigeration*, **98**, 161-170 (2019). https://doi.org/10.1016/j.ijrefrig.2018.09.003
9. M. M. Younes, I. I. El-Sharkawy, A. E. Kabeel, K. Uddin, T. Miyazaki, and B. B. Saha, *International Journal of Refrigeration*, **118**, 345-353 (2020). https://doi.org/10.1016/j.ijrefrig.2020.04.002
10. M. Jafari, G. R. Najafi, M. A. Sharif, and Z. Elyasi, *Polymers and Polymer Composites*, **29**, 563-826 (2021). https://doi.org/10.1177/0967391120933482
11. L. Liu, H. Huang, Z. He, S. Li, J. Li, and J. Chen, *Nanoscale and Microscale Thermophysical Engineering*, **22**, 255-269 (2018). https://doi.org/10.1080/15567265.2018.1490938
12. S. D. White, M. Goldsworthy, R. Reece, T. Spillmann, A. Gorur, and D.-Y. Lee, *International Journal of Refrigeration*, **34**, 1786-1791 (2011). https://doi.org/10.1016/j.ijrefrig.2011.06.012
13. S. De Antonellis, E. Bramanti, L. Calabrese, B. Campanella, and A. Freni, *Applied Thermal Engineering*, **214**, 118857 (2022). https://doi.org/10.1016/j.applthermaleng.2022.118857
14. A. S. Alsaman, E. M. M. Ibrahim, M. S. Ahmed, E. S. Ali, A. M. Farid, and A, A. Askalany, *Energy Conversion and Management*, **266**, 115818 (2022). https://doi.org/10.1016/j.enconman.2022.115818
15. X. Chen, Z. Niua, J. Wang, G. R. Zhu, and M. Zhou, *Ceramics International*, **44**(15), 18173-18180 (2018). https://doi.org/10.1016/j.ceramint.2018.07.025
16. M. Li and Z. Wu, *Journal of Macromolecular Science, Part B: Physics*, **51**, 1647-1657 (2012). http://dx.doi.org/10.1080/00222348.2012.657126
17. S. Belguith, Z. Meddeb, and R. B. Slama, *Science and Technology for the Built Environment*, **27**, 1368-1380 (2021). https://doi.org/10.1080/23744731.2021. 1944666
18. R. H. Galib, Y. Tian, Y. Lei, S. Dang, X. Li, A. Yudhant, G. Lubineau, and Q. Gan, *Nature Communications*, **14**(1), 6707 (2023). https://doi.org/10.1038/s41467-023-42548-0
19. C.-H. Chen, C.-Y. Hsu, C.-C. Chen, Y.-C. Chiang, and S.-L. *Chen, Energy*, **94**, 87-99 (2016). https://doi.org/10.1016/j.energy.2015.10.139
20. W. Zhang, P. Wang, S. Liu, J. Chen, R. Chen, X. He, G. Ma, and Z. Lei, *Journal of Material Science*, **56**, 16223-16242 (2021). https://doi.org/10.1007/s10853-021-06306-1
21. A. Taher and H. J. H. Brouwers, *Construction and Building Materials*, **379**, 131166 (2023). https://doi.org/10.1016/j.conbuildmat.2023.131166
22. F. Rom'an, D. O. Mbuge, and O. Hensel, *Drying Technology*, **37**(11), 1441-1453 (2018). https://doi.org/10.1080/07373937.2018.1504063
23. Y. Xue, Q. Li, R. Wang, and T. Ge, *International Journal of Refrigeration*, **158**, 385-392 (2024). https://doi.org/10.1016/j.ijrefrig.2023.12.003
24. Fr. Comino, P. E. Romero, E. Molero, and M. R. de Adana, *Applied Thermal Engineering*, **227**, 120393 (2023). https://doi.org/10.1016/j.applthermaleng.2023.120393
25. M. Thommes, K. Kaneko, A. V. Neimark, J. P. Olivier, F. Rodriguez-Reinoso, J. Rouquerol, and K. S. W. Sing, *Pure Applied Chemistry*, **87**, 1051-1069 (2015). https://doi.org/10.1515/pac-2014-1117